Impact of shrubs on surface albedo and snow specific surface area at a low arctic site: in-situ measurements and simulations

M. Belke-Brea, Florent Domine, M. Barrere, G. Picard, L. Arnaud

Impact of Shrubs on Winter Surface Albedo and Snow Specific Surface Area at a Low Arctic Site: In Situ Measurements and Simulations

M. BELKE-BREA

Takuvik Joint International Laboratory, Université Laval and CNRS-INSU, and Centre d'Études Nordiques, and Department of Geography, Université Laval, Québec City, Quebec, Canada

F. DOMINE

Takuvik Joint International Laboratory, Université Laval and CNRS-INSU, and Centre d'Études Nordiques, and Department of Chemistry, Université Laval, Québec City, Quebec, Canada

M. BARRERE

Takuvik Joint International Laboratory, Université Laval and CNRS-INSU, and Centre d'Études Nordiques, and Department of Geography, Université Laval, Québec City, Quebec, Canada, and Météo-France–CNRS, CNRM UMR 3589, CEN, Grenoble, France

G. PICARD AND L. ARNAUD

Université Grenoble Alpes, CNRS, IRD, Grenoble INP, IGE, Grenoble, France

(Manuscript received 30 April 2019, in final form 29 August 2019)

ABSTRACT

Erect shrubs in the Arctic reduce surface albedo when branches protrude above the snow and modify snow properties, in particular specific surface area (SSA). Important consequences are changes in the land surface–atmosphere energy exchange and the increase of snow melting in autumn, possibly inducing reduced soil thermal insulation and in turn permafrost cooling. Near Umiujaq (56.5°N, 76.5°W) in the Canadian low Arctic where dwarf birches (*Betula glandulosa*) are expanding, spectral albedo (400–1080 nm) under diffuse light and vertical profiles of SSA were measured in November and December 2015 at four sites: three with protruding branches and one with only snow. At the beginning of the snow season (8 November), shrub-induced albedo reductions were found to be wavelength dependent and as high as 55% at 500 nm and 18% at 1000 nm, which, integrated over the measurement range (400–1080 nm), corresponds to 70 W m^{-2} of additional absorbed energy. The impact of shrubs is not just snow darkening. They also affect snow SSA in multiple ways, by accumulating snow with high SSA during cold windy precipitation and favoring SSA decrease by inducing melting during warm spells. However, the impact on the radiation budget of direct darkening from shrubs likely dominates over the indirect change in SSA. Spectral albedo was simulated with a linear mixing equation (LME), which fitted well with observed spectra. The average root-mean-square error was 0.009. We conclude that LMEs are a suitable tool to parameterize mixed surface albedo in snow and climate models.

1. Introduction

With climate warming, shrubs are expanding on the Arctic tundra (Tape et al. 2006; Myers-Smith et al. 2011; Ropars and Boudreau 2012), changing its winter surface from undisturbed snow to a mixed surface of snow and protruding branches. This mixed surface has a lower albedo in the visible (380–750 nm) than undisturbed snow (Sturm et al. 2005; Loranty et al. 2011) positively feeding back on regional and global climate warming (Sturm et al. 2001; Loranty and Goetz 2012). Quantifying the shrub–albedo feedback and its impact on future climate can be done by implementing parameterizations of mixed surface albedo in climate models (Bonfils et al. 2012; Loranty and Goetz 2012; Pearson et al. 2013). A commonly used

Denotes content that is immediately available upon publication as open access.

Corresponding author: Florent Domine, florent.domine@gmail.com

DOI: 10.1175/JCLI-D-19-0318.1

parameterization is a linear mixing equation (LME) (Sturm et al. 2005; Marsh et al. 2010) where mixed surface albedo α_{mix_calc} is calculated by weighting snow albedo α_{sn} and shrub albedo α_{veg} proportionally to the surface area covered by each:

$$\alpha_{mix\_calc} = (1 - \chi)\alpha_{sn} + \chi\alpha_{veg}, \quad (1)$$

where χ is a weighting factor. Despite its common application, the performance of this parameterization has only been validated with broadband albedo measurements (Sturm et al. 2005; Ménard et al. 2014) and has never been tested for spectral albedo due to the lack of validation data since, to our knowledge, spectral albedo has never been measured from the ground over mixed surfaces in the Arctic. Multispectral reflectance measurements from satellites are available, but their use for testing albedo data is delicate since mixed surfaces are not Lambertian.

Shrub–albedo spectra α_{veg} are easy to obtain because they can be measured directly in the field in autumn after leaf fall but before snowfall and used in winter since branch albedo is consistent throughout the year. However, it is more complicated to determine the snow-only albedo spectra α_{sn} in the presence of shrubs because, albedo being hemispherically integrated, the footprint of a sensor inevitably comprises protruding branches and albedo measurements can thus only record the mixed reflectance of snow and protruding branches. Contact probes could be attempted but they measure directional reflectance rather than albedo (Painter et al. 2007) and their size is often too large for the dense branch network encountered. Measuring α_{sn} over adjacent shrub-free sites is not necessarily a solution because protruding branches can locally modify the physical properties of snow, which in turn affect snow albedo.

The main snow physical property that influences albedo and is affected by shrubs is the snow specific surface area (SSA), which is simply related to the optical grain diameter d_{opt} by

$$SSA = \frac{6}{\rho_{ice} d_{opt}}, \quad (2)$$

where ρ_{ice} is the ice density, 917 kg m^{-3} at 0°C (Warren 1982; Domine et al. 2007). Snow with larger SSA scatters light more efficiently and thus has a higher albedo, especially in the near-infrared spectrum (750–2500 nm) (Warren 1982). Fresh snow has the highest SSA, but this parameter changes continuously in space and over time because of snow metamorphism, which modifies the size and shape of snow grains (Taillandier et al. 2007).

At the surface, the principal drivers for snow metamorphism are meteorological variables, mostly wind speed and temperature. For air temperatures <0°C, wind accelerates the decrease in SSA of fresh snow (Cabanes et al. 2003) but can increase the SSA of aged snow (Domine et al. 2009). Shrubs reduce wind speed at the ground surface, causing snow to accumulate there (Sturm et al. 2001; Liston et al. 2002; Essery and Pomeroy 2004; Pomeroy et al. 2006; Marsh et al. 2010; Domine et al. 2016). For air temperature >0°C, snow melting leads to very low SSA values (Domine et al. 2007). Melting is accelerated by the presence of shrubs because branches with low albedo absorb light, heat up, and emit radiation in the thermal infrared, causing the surrounding snow to melt (Sturm et al. 2005; Pomeroy et al. 2006; Marsh et al. 2010; Barrere et al. 2018). Shrub-induced increases in snow accumulation and melting likely cause snow SSA, and therefore albedo, in mixed surfaces to be different from that of shrub-free tundra. In those cases accurate α_{sn} spectra can only be obtained by computing them as a function of measured SSA rather than by measuring them over shrub-free sites.

In this study we present the first ground-based spectral albedo measurements (400–1080 nm), taken over mixed surfaces of snow and dwarf birches (*Betula glandulosa*) near Umiujaq, northern Quebec. We used the measured spectra to determine the suitability of the commonly used LME to simulate spectral albedo of mixed surfaces. We also test the sensitivity of the LME performance to the choice of α_{veg} by using four different input spectra. Finally, we test whether computing α_{sn} as a function of measured SSA improves the performance and accuracy of the LME in predicting albedo compared to simulations where α_{sn} was derived from snow albedo measurements at an adjacent pure snow site. With this study we want to test the suitability of the LME to calculate albedo of mixed surfaces with snow and shrubs and we hope to contribute to a better understanding of the complex shrub–snow–albedo interactions, which would allow a more accurate quantification of the shrub–albedo feedback.

2. Methods

a. Study sites

The research area is located in the low Arctic in the glacier-shaped Tasiapik Valley next to the village of Umiujaq in northern Quebec (Fig. 1). An automatic weather station (AWS) records hourly averages of meteorological variables in the valley since 1997. The mean annual air temperature (1997–2015) is −3°C (CEN 2016). Snowstorms are frequent from October until December, and wind speeds can reach 22 m s^{-1}

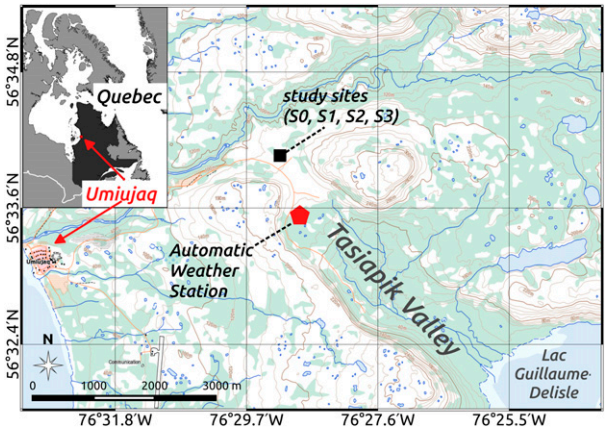

FIG. 1. Location of study sites and automatic weather station in the Tasiapik Valley near Umiujaq in northern Quebec, Canada. Map source: Natural Resources Canada (http://atlas.gc.ca/toporama/en/index.html).

during these events. For the 2012–15 period, around 20% of recorded wind speeds exceeded 5 m s^{-1} (CEN 2016), the approximate threshold for snow drifting (Vionnet et al. 2013).

The Tasiapik Valley lies in the forest-tundra ecotone (Payette 1976), which is characterized by trees in wind-sheltered depressions and lichen and shrubs of varying height covering the wind-exposed uplands (Grégoire and Bégin 1993). The main shrub species are dwarf birch (*Betula glandulosa*) and willow (mostly *Salix glauca* and *S. planifolia*), which have been expanding and replacing lichen patches of mostly *Cladonia spp.* in the last decade (Ropars and Boudreau 2012; Provencher-Nolet et al. 2014). For this study, we selected four sites located on the upper part of the Tasiapik Valley (Fig. 1). The first (S0) is a lichen site and the three others are characterized by *Betula glandulosa* shrubs of different heights: ~36 cm (S1), ~80 cm (S2), and ~120 cm (S3). The four sites lay within 50 m of each other and had similar topographical and meteorological conditions.

b. Experimental methods

1) Overview

Field work took place during two campaigns, one in late summer (September) and one in autumn (late October to December) 2015. The late summer campaign was conducted to acquire spectral albedo over shrubs (α_{veg}) before the start of the snow season but after most leaves had already fallen. Later, during the autumn campaign, we designated the four study sites (S0 in lichen and S1–S3 in shrubs) where we measured time series of spectral albedo (α_{sn_obs} at S0 and α_{mix_obs} at S1–S3). We also measured SSA for snow albedo computations (α_{sn_TARTES}) for which we used the Two-Stream Radiative Transfer in Snow model (TARTES; Libois et al. 2013).

2) Spectral albedo measurements

Spectral albedo was calculated as the ratio of spectral reflected over incident radiation that were measured with the Solalb instrument. Solalb is a simpler and mobile version of the Autosolexs instrument described in Picard et al. (2016b). Basically it consists of a cosine light collector, which is attached to one end of a 2 m long, rotatable metallic arm. Incident and reflected radiation are captured by orienting the metallic arm toward the sky and toward the ground, respectively. However, since they are not measured simultaneously, incoming radiation can fluctuate during the acquisition period, particularly during overcast conditions. Fluctuations were monitored by a photodiode and measurements for which fluctuations exceeded 1% were discarded. The leveling of the instrument during data acquisition is critical within 0.2° and was measured by an electronic inclinometer attached close by the cosine collector. Radiation was captured by the light collector and transmitted through an optical fiber to a MayaPro spectrometer from Ocean Optics that has an effective resolution of 3 nm and a spectral range from 200 to 1120 nm. However, we only used the 400 to 1080 nm range because data in 200 to 400 nm and 1080 to 1120 nm ranges had a low signal-to-noise ratio and were discarded. A first-order Butterworth filter was applied to all spectra to remove variations with intensity amplitudes of 0.05 or lower. The Butterworth filter was provided by the Python scipy.signal.butter function and used with a cutoff frequency of 0.05.

A detailed description of the design and characterization of the home-built Solalb's light collector can be found in Picard et al. (2016b). It is important to note that the collector's response for radiation with a zenith angle >70° introduces an uncorrectable error of ±15% to the measurements (Picard et al. 2016b). This is problematic because in the Arctic, in autumn and winter, solar zenith angles are generally larger than 70°. To avoid such errors, measurements were only taken during overcast conditions, when radiation is coming from every direction in the sky, and with a maximal contribution around 45° in zenith angle, a range where the cosine collector is excellent. These conditions also greatly limit the impact of the surface slope (Lee et al. 2011).

3) SSA measurements

Snow SSA was measured together with spectral albedo at each of the four study sites. It was measured in the upper 10 cm of the snowpack along vertical profiles with a 1 cm resolution using the Dual Frequency Integrating Sphere for Snow SSA Measurement (DUFISSS) instrument detailed

in Gallet et al. (2009). Briefly, infrared reflectance of snow samples is measured at 1310 nm using an integrating sphere and SSA is calculated from that reflectance with a fairly simple algorithm.

To model snow albedo of a multilayer snowpack with TARTES, it is necessary to know the snow density profiles in addition to the SSA profiles of the snowpack (Libois et al. 2013). However, density could not be measured in the field due to short measuring days and harsh measuring conditions. Instead, based on 5 years of simultaneous measurements of density and SSA at this site, we determined an SSA–density correlation for surface snow, similar to the approach of Domine et al. (2007), which we used to estimate density. The correlation is shown in Fig. 2.

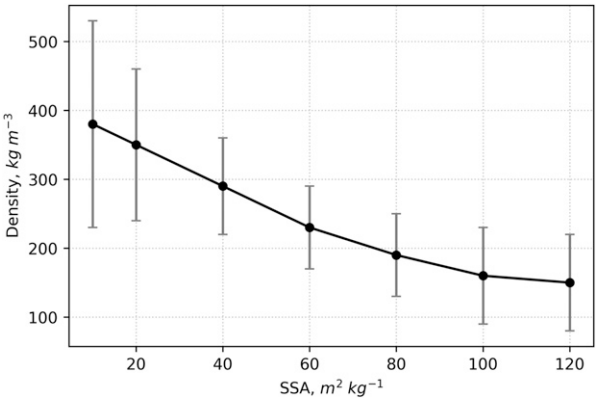

FIG. 2. Empirical correlation of snow density and SSA for surface snow based on 5 years of snow measurements near Umiujaq.

4) ALBEDO CALCULATIONS FROM SSA MEASUREMENTS

TARTES is a radiative transfer model that allows the determination of snow albedo of a multilayered snowpack with known snow physical properties (Libois et al. 2013) (it is available from https://pypi.org/project/tartes/). We use the updated ice absorption spectrum from Picard et al. (2016a), which is higher in the visible range than in Warren and Brandt (2008). Every snow layer with a given thickness is characterized by its SSA, which we measured, and by snow density, which was determined with the empirical correlation shown in Fig. 2. Layer thickness was set to 1 cm, the resolution of the SSA profiles, except for the bottom layer, which was set to 1000 cm to exclude influence of underlying soil. Illumination conditions were set to 100% diffuse.

c. *Measured albedo correction*

The comparison between measured and simulated albedo can be biased because measured albedo is often subject to artifacts such as variations in illumination, shadows cast by the instrument and operator, slopes of the surface, etc. To account for these wavelength-independent artifacts, we followed the approach of Picard et al. (2016b) and introduced a free, wavelength-independent scaling factor A, which was used to correct observed albedo ($\alpha_{\text{mix\_obs}}$):

$$\alpha_{\text{mix\_obs,corr}}(\lambda) = A^{-1}\alpha_{\text{mix\_obs}}(\lambda). \quad (3)$$

The scaling factor A was obtained by calculating a theoretical, artifact-free snow albedo ($\alpha_{\text{sn\_TARTES}}$) for the pure snow site S0 using measured SSA, estimated density (see Fig. 2) and the radiative transfer model TARTES. A was retrieved by fitting $\alpha_{\text{sn\_TARTES}}$ and $\alpha_{\text{sn\_obs}}$ using a linear least squares method (provided by the Python scipy.optimize.least_squares function), which minimizes the squared difference between $\alpha_{\text{sn\_TARTES}}$ and $\alpha_{\text{sn\_obs}}$. Assuming A is the same for all measurements taken on a given day, the values retrieved for S0 can then be used to correct the observed spectra at shrub sites S1–S3.

d. *Simulating mixed surface albedo with an LME*

To investigate the suitability of the LME [Eq. (1)] to simulate mixed surface albedo ($\alpha_{\text{mix\_calc}}$), we designed a modeling approach where we consider α_{sn} and α_{veg} to be known parameters and the proportion parameter χ to be adjustable. The best-fitting χ is retrieved by matching $\alpha_{\text{mix\_calc}}$ to the corrected spectra measured at the shrub sites ($\alpha_{\text{mix\_obs,corr}}$). The fit is performed with a linear least squares method and the performance of the LME is assessed by determining the fit quality between $\alpha_{\text{mix\_calc}}$ and $\alpha_{\text{mix\_obs,corr}}$, that is, the root-mean-square error (RMSE).

The performance of the model was tested for four α_{veg} spectra. The first was an average of five measurement taken with Solalb near Umiujaq during the summer campaign in 2015 over dwarf birches (*Betula glandulosa*) with various understories, that is, moss, lichen, and dead leaves (see the appendix, Fig. A1). The average has a low maximal standard variation of 0.01 in the visible (400–750 nm) and 0.02 in the near-infrared (750–1080 nm) suggesting that different types of understory had little influence on albedo. In addition to the Umiujaq spectrum ($\alpha_{\text{veg\_umi}}$), we used two spectra from Juszak et al. (2014) who employed a contact probe to measure branch reflectivity of young ($\alpha_{\text{veg\_}y}$) and old ($\alpha_{\text{veg\_}o}$) dwarf birches (*Betula nana*) in Siberia. For the fourth spectrum, we calculated the average of $\alpha_{\text{veg\_}y}$ and $\alpha_{\text{veg\_}o}$ to obtain a mixed reflectivity of young and old branches ($\alpha_{\text{veg\_}y+o}$). Figure 3 depicts the four different spectra.

To calculate α_{sn} in mixed surfaces with TARTES we had to make the following assumptions: 1) SSA at each

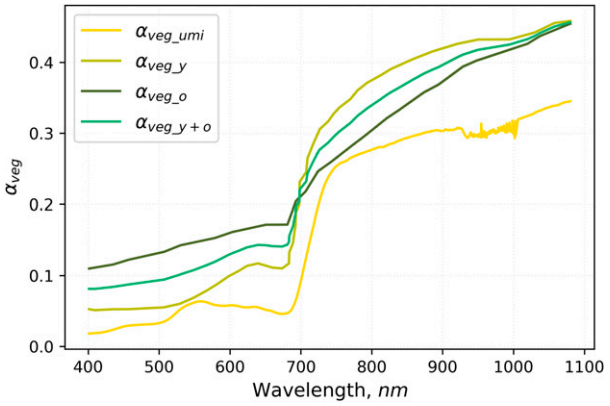

FIG. 3. Four shrub albedo spectra used as α_{veg} input parameter for simulations with the LME [Eq. (1)]. The spectra include 1) the average of five albedo spectra measured in late summer 2015 near Umiujaq (α_{veg_umi}) over *Betula glandulosa* shrubs, 2) two measurements conducted by Juszak et al. (2014) with a contact probe in Siberia for young (α_{veg_y}) and old (α_{veg_o}) branches of *Betula nana* shrubs, and 3) one average spectra of Juszak's young and old branch spectra (α_{veg_y+o}).

site is relatively homogeneous and the measured profiles are therefore representative for the entire area of the site. 2) Snow SSA and density are correlated, so the profile of the latter can be deduced from the measured profiles of SSA (Fig. 2). 3) The impurity content is negligible and assumed to be zero. 4) Illumination conditions were always 100% diffuse. These assumptions allow calculating a theoretical albedo α_{sn_TARTES} for each shrub site and day of albedo measurements.

An alternative approach is to use snow albedo measured over shrub-free surfaces and to simply assume that snow albedo in mixed and pure snow surfaces resemble each other enough to be considered the same. To test this second approach, an additional simulation was run with the measured snow albedo from the S0 lichen site (α_{sn_obs}).

3. Results

a. Spectral albedo of mixed and pure snow surfaces

Adding up the four study sites we obtained 49 valid spectral albedo measurements. Representative spectra for each site are shown in Fig. 4 for 8 November, 22 November, and 2 December. Over that period, snow depth at S2 and S3 increased from around 40 to 69 cm (S2) and 79 cm (S3), decreased slightly from 35 to 24 cm at S1 and remained steadily around 20 cm at S0 (Table 1). Shrub-induced albedo decreases were wavelength dependent and more pronounced in the visible spectrum than in the near-infrared spectrum (Fig. 4). For example, on 8 November, the albedos at 500 nm for S0 and S3 were 0.92

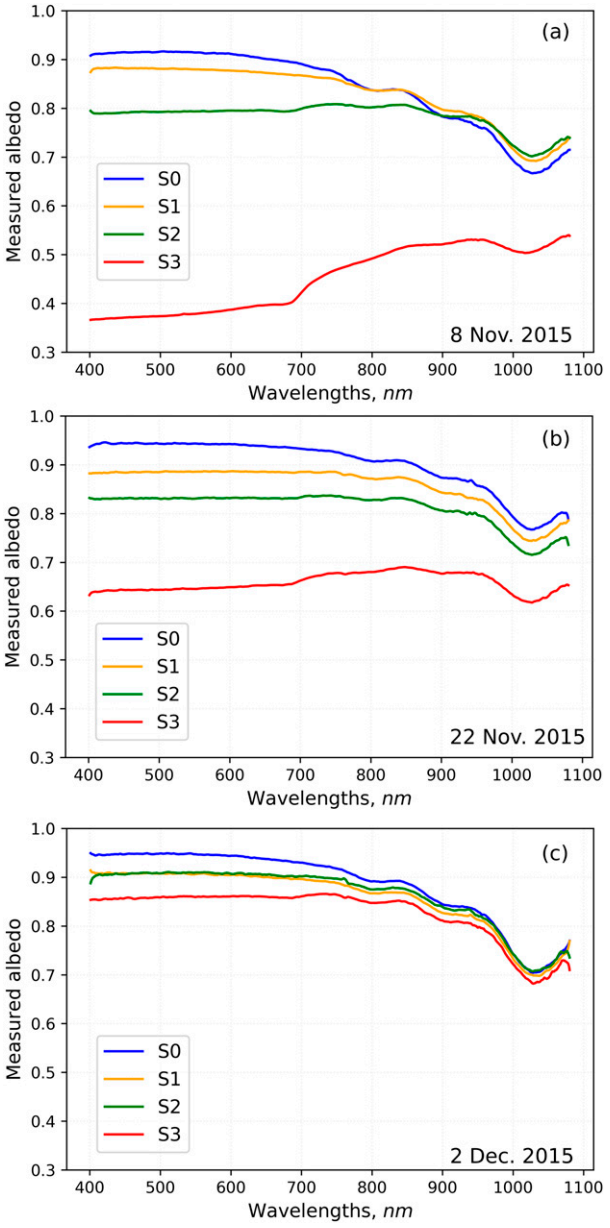

FIG. 4. Comparison of spectral albedo measured in Umiujaq on (a) 8 Nov, (b) 22 Nov, and (c) 2 Dec 2015 at four different sites (S0–S3). S0 is a lichen site with a pure snow surface, S1–S3 are shrub sites with shrubs of different heights: ~36 cm (S1), ~80 cm (S2), and ~120 cm (S3).

and 0.37, respectively, representing an albedo reduction of 55%. On the other hand, at 1000 nm measured albedo was 0.69 for S0 and 0.51 for S3, representing a reduction of only 18%. Albedo in the visible at S2 and S3 increased gradually in the time span from 8 November to 2 December. On 2 December, albedos in the visible at all sites were still within 10%, meaning that the formation of a highly reflective pure snow surface at S2 and especially at S3 was

TABLE 1. Snow depth in cm at the lichen site S0, small shrub site S1 (~36 cm), the medium shrub site S2 (~80 cm), and the tall shrub site S3 (~120 cm). Snow depth was measured with a snowprobe.

Date	S0	S1	S2	S3
8 Nov 2015	15	35	40	44
22 Nov 2015	21	29	56	65
2 Dec 2015	15	24	69	79

delayed by more than a month compared to the lichen site S0. Comparing S1 and S0, spectra were within 6% throughout the study, showing that small shrubs of ~36 cm had a limited effect on albedo.

b. *Shrub–snow–SSA interactions under different meteorological conditions*

Weather in autumn 2015 was characterized by strong winds, warm spells, or a combination of both, as detailed in Barrere et al. (2018). During those meteorological conditions, shrubs had a visible effect on the surface snow layer (Fig. 5). Warm spells caused extensive snow melting around protruding branches (Fig. 5a) while windy conditions caused the preferential accumulation of wind-blown snow around shrubs, forming distinct snow mounds (Fig. 5b), whereas shrub-free areas retained a hard and icy surface.

After warm spells or windy conditions, SSA profiles (0 to −10 cm from surface) varied between mixed and pure snow surfaces. Figure 6 shows SSA profiles for S0, S1, S2, and S3 measured on 8 November, 15 November, and on 22 November, each day preceded by different meteorological conditions. Before 8 November, air temperatures were above freezing, it rained, and winds were strong (6 and 7 November). In the night from 7 to 8 November there was a blizzard during which temperatures dropped to −5°C. On 8 November, wind calmed down, temperatures varied between −2° and −5°C, and there was sunshine in the morning and light precipitation in the afternoon. SSA profiles were measured in the afternoon of 8 November (Fig. 6a) and show very low values at S3 (5–15 $m^2 kg^{-1}$) but high values in the upper 4 cm at S2 (35–62 $m^2 kg^{-1}$). At S0 only SSA at 0 cm is high (42 $m^2 kg^{-1}$), the rest of the profile has values similar to S3. Instrument problems prevented SSA measurements at S1 on 8 November. The highest wind speeds of the season (16 $m s^{-1}$) were measured during a blizzard on 13 and 14 November during which temperatures increased from −10°C to −5°C. SSA measured on 15 November at shrub sites S1, S2, and S3 had significantly higher surface values (60–78 $m^2 kg^{-1}$, Fig. 6b) than SSA at S0 (10 $m^2 kg^{-1}$), where snow had been eroded down to an icy layer. Before 22 November, temperatures were below freezing, and fresh snow precipitated without wind and the SSA profiles had similarly high values at all sites (64–89 $m^2 kg^{-1}$; Fig. 6c).

c. *Retrieval of scaling factor A*

Scaling factors were retrieved for 13 S0 albedo measurements (α_{sn_obs}) using theoretical snow albedo (α_{sn_TARTES}) calculated with TARTES and the vertical SSA profiles obtained at S0 for every measuring day. Figure 7a highlights how measured albedo (α_{sn_obs}, black) had lower values than the theoretical spectra (α_{sn_TARTES}, red) due to the influence of artifacts.

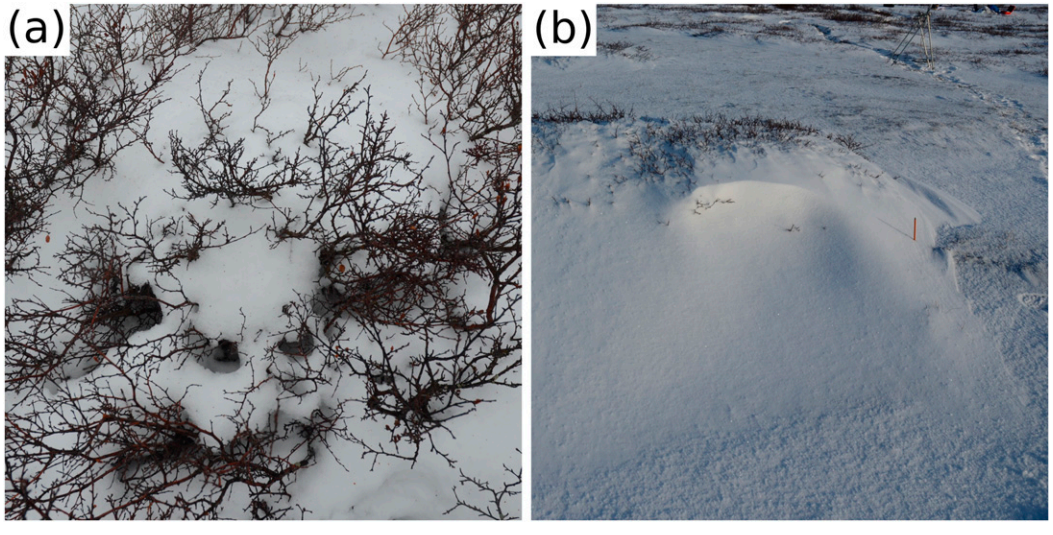

FIG. 5. Photographs taken during the autumn campaign illustrating snow–wind–melting interactions. (a) increased melting in shrubs during the warm spell on 6 and 7 Nov, and (b) accumulation of wind-drifted snow in and around shrubs on 15 Nov.

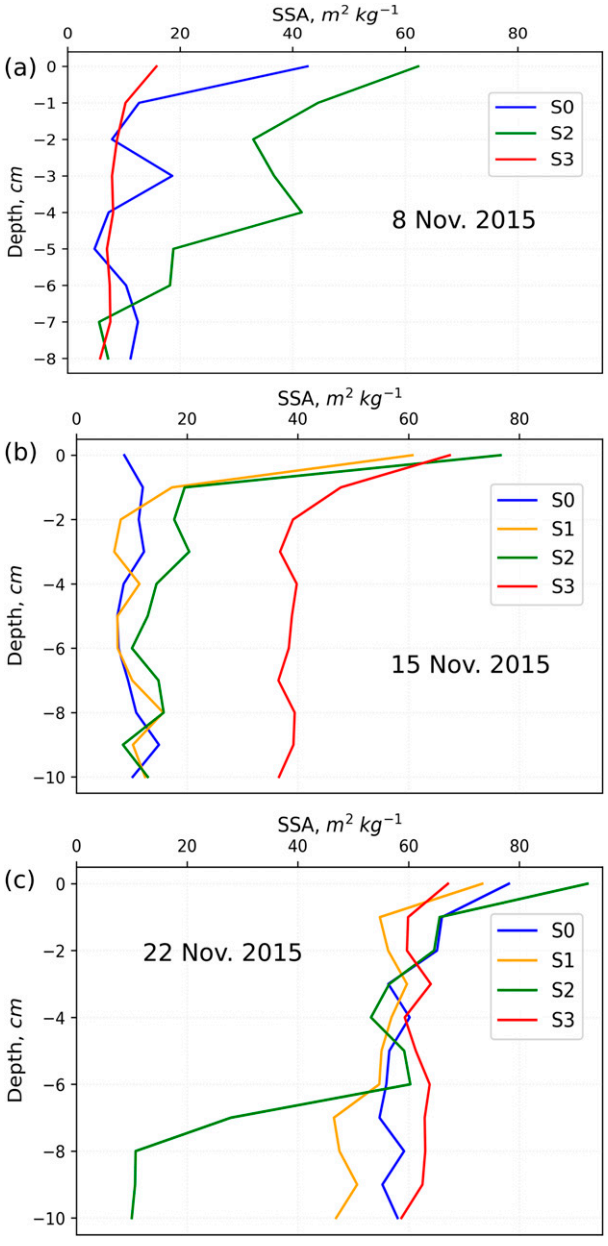

FIG. 6. SSA profiles measured for the upper 10 cm of the snowpack near Umiujaq on (a) 8 Nov, (b) 15 Nov, and (c) 22 Nov 2015 at the four different study sites S0 to S3. Different meteorological conditions preceded the three days: before the 8 Nov temperatures were close to 0°C, and we observed melting. Before 15 Nov wind speeds were extremely high (16 m s^{-1}) and temperatures significantly below 0°C. On 22 Nov snow precipitated under cold and calm conditions. Instrument problems prevented SSA acquisition at S1 on 8 Nov.

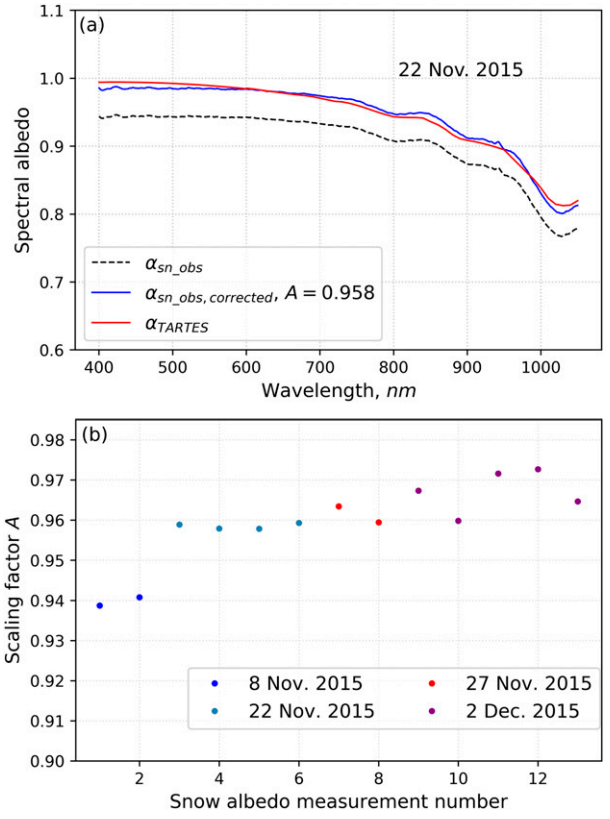

FIG. 7. Determination of the scaling factors used to correct artifacts in measured albedo. (a) α_{sn_obs} (black) is the spectral snow albedo measured at the lichen site S0 on 22 Nov. α_{sn_TARTES} (red) is the theoretical snow albedo computed with TARTES from the SSA profiles. $\alpha_{sn\_obs,corrected}$ (blue) is the measured spectrum after correction with $A = 0.958$. (b) Deduced scaling factors for all 13 snow albedo measurements taken at S0 during the autumn campaign 2015 in Umiujaq.

Introducing A allowed the correction of α_{sn_obs} so that it matched the theoretical spectrum α_{sn_TARTES} ($\alpha_{sn\_obs,corr}$, blue). The fits achieved between the 13 corrected and theoretical spectra ($\alpha_{sn\_obs,corr}$ and α_{sn_TARTES}) were good and had a mean RMSE of 0.013. The retrieved A values are plotted in Fig. 7b; they were similar for all days and ranged between 0.96 and 0.97, except for the 8 November when values were around 0.94. To correct albedo measured over mixed surfaces (α_{mix_obs}), we used the mean A value averaged for every measuring day.

d. LME simulations

The performance of the LME was tested with 36 $\alpha_{mix\_obs,corr}$ spectra and, in most cases, returned a good fit between observed and simulated albedo. In most cases the RMSE varied significantly with the choice of α_{veg} and best fits were usually obtained with the branch reflectivity measurements of Juszak et al. (2014). Figure 8 shows four examples to present the fits achieved between observed (black) and simulated (red) spectra with the best-fitting α_{veg}, and also to present the variations introduced by the choice of α_{veg} (blue, green, and yellow). Naturally, those variations were more pronounced in tall shrubs (S3) and

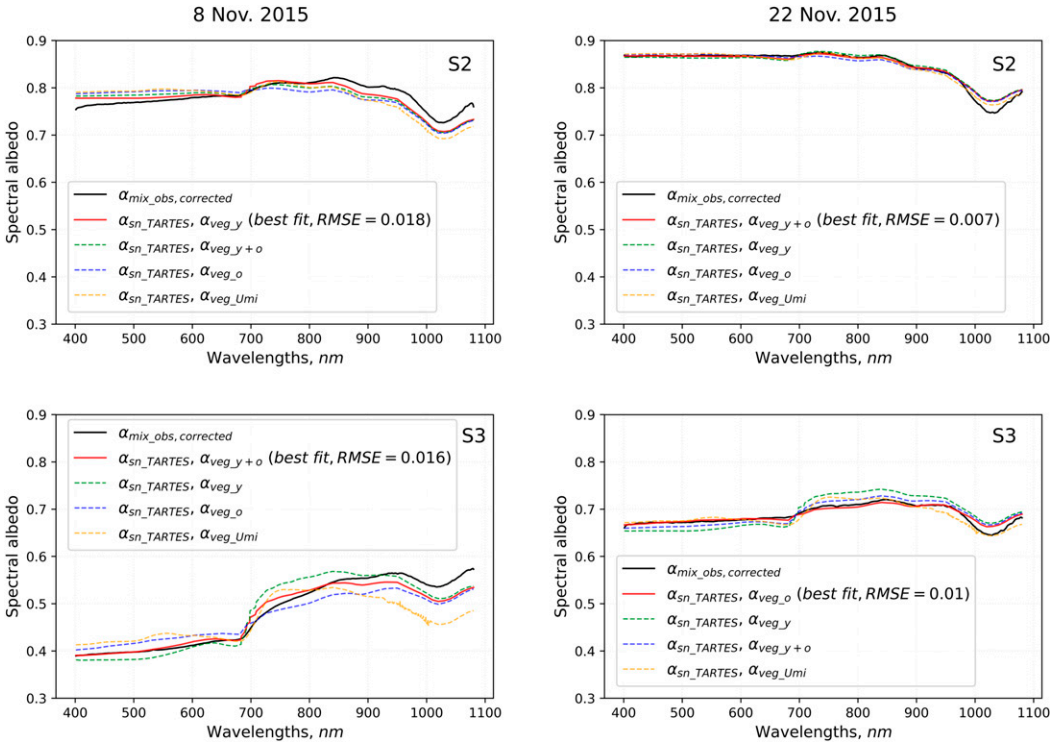

FIG. 8. Illustrations of the fit between observed albedo at shrub sites S2 and S3 ($\alpha_{mix\_obs,corrected}$, black) and simulations with the LME [Eq. (1)]. Simulations in red used the best-fitting α_{veg} spectra, all other colors (green, blue, and yellow) are simulations with alternative α_{veg} spectra. α_{veg_o} and α_{veg_y} are old and young branch reflectivity (Juszak et al. 2014), α_{veg_y+o} is the average spectra of old and young branches and α_{veg_umi} is the average of five albedo spectra measured near Umiujaq. All simulations used snow albedo computed with TARTES (α_{sn_TARTES}).

early in the snow season (8 November) because of the proportionally larger contribution of α_{veg} to the total surface albedo. All simulations in Fig. 8 were run with snow albedo spectra obtained with TARTES (α_{sn_TARTES}).

Variations induced by the two approaches for snow albedo estimation, that is, calculation with TARTES (α_{sn_TARTES}) versus measurements at S0 (α_{sn_obs}), were surprisingly small for most days and the average RMSE was only slightly better for simulations using α_{sn_TARTES} (0.009) than for those using α_{sn_obs} (0.012). The RMSE was only averaged for simulations made with the best-fitting α_{veg}. To analyze the impact of the two approaches at different wavelengths, we calculated the residuals per wavelength between the 36 observed spectra and the corresponding simulations run with α_{sn_TARTES} and α_{sn_obs}, respectively, and show their average in Fig. 9. For both cases, mean residuals were similar at most wavelengths, but the standard deviation, indicated by the red and blue shaded areas in the graph (Fig. 9), were larger for simulations using α_{sn_obs}, especially in the range 950–1080 nm. Those large variations were caused by simulations for days when SSA values for mixed and pure snow surfaces were different, such as on 8 November, because this is when the simplified approach (using α_{sn_obs}) cannot return accurate snow albedo spectra reducing LME performance (i.e., larger residuals).

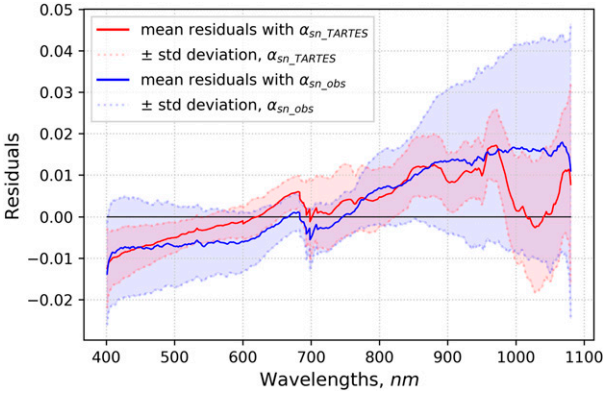

FIG. 9. Average residuals (solid line) and their standard deviation (dashed line and shaded area) per wavelength for LME simulations conducted with a snow albedo parameter computed with TARTES (α_{sn_TARTES}, red) and a snow albedo parameter derived from snow albedo measurements at S0 (α_{sn_obs}, blue).

4. Discussion

a. Impact of shrubs on spectral mixed surface albedo

In the visible spectrum (400–750 nm) where branches are highly absorbent (albedo 0.05–0.1, Fig. 3), and snow highly reflective, shrubs strongly reduced albedo by up to 55% compared to pure snow surfaces where albedo was almost 1 (S3 vs S0 in Fig. 4a). In the near-infrared spectrum (750–1080 nm), branches are less absorbent (albedo around 0.4, Fig. 3) and pure snow less reflective (albedo generally 0.55–0.85), shrub-induced albedo reductions were therefore only up to 18% (S3 vs S0 in Fig. 4a). A peculiarity on 8 November is the higher near-infrared albedo at S2 than at S0. The increase is probably produced by the higher snow SSA due to the recent snowfall, and hence reflectance, at S2 (Fig. 6a), which counterbalanced the absorption of protruding branches.

Overall, however, shrub-induced albedo reductions were significant and, at S3, delayed most of the surface brightening associated with the formation of a pure snow layer by a full month, which has an important impact on the tundra surface shortwave radiation budget. To quantify the amount of absorbed radiation at S0, S2, and S3 on 8 November and 2 December we multiplied incoming radiation with measured spectral albedo. Incoming radiation was not taken from Solalb measurements because we did not conduct an absolute calibration of the spectrometer signal. Instead, it was determined with SBDART, a model that computes plane-parallel radiative transfer in Earth's atmosphere (Ricchiazzi et al. 1998). Here, the model atmosphere was set to the implemented version for subarctic winter and a cloud layer was introduced stretching from 1 to 2 km height with an optical thickness of 4 at 550 nm to simulate overcast measuring conditions. Incoming radiation for 8 November and 2 December at local noon are shown in Fig. 10a and spectra of absorbed energy for S0, S2, and S3 are shown in Fig. 10b (8 November) and Fig. 10c (2 December). On 8 November and compared to S0, additionally absorbed energy integrated over 400–1080 nm was 70 W m^{-2} at S3 and 13 W m^{-2} at S2, which are significant for the surface energy budget. On 2 December this amount was reduced to 6 and 2 W m^{-2} at S3 and S2, respectively, due to the lower amount of protruding branches because of increased snow depth and because of the smaller amount of incoming radiation. Since the spectrometer used in this study registers radiation only up to 1080 nm, the values calculated here are a lower limit of additional absorption and calculations considering the entire solar spectrum should return even higher values.

In addition to the overall impact on the surface energy budget, potentially important effects arise from the fact

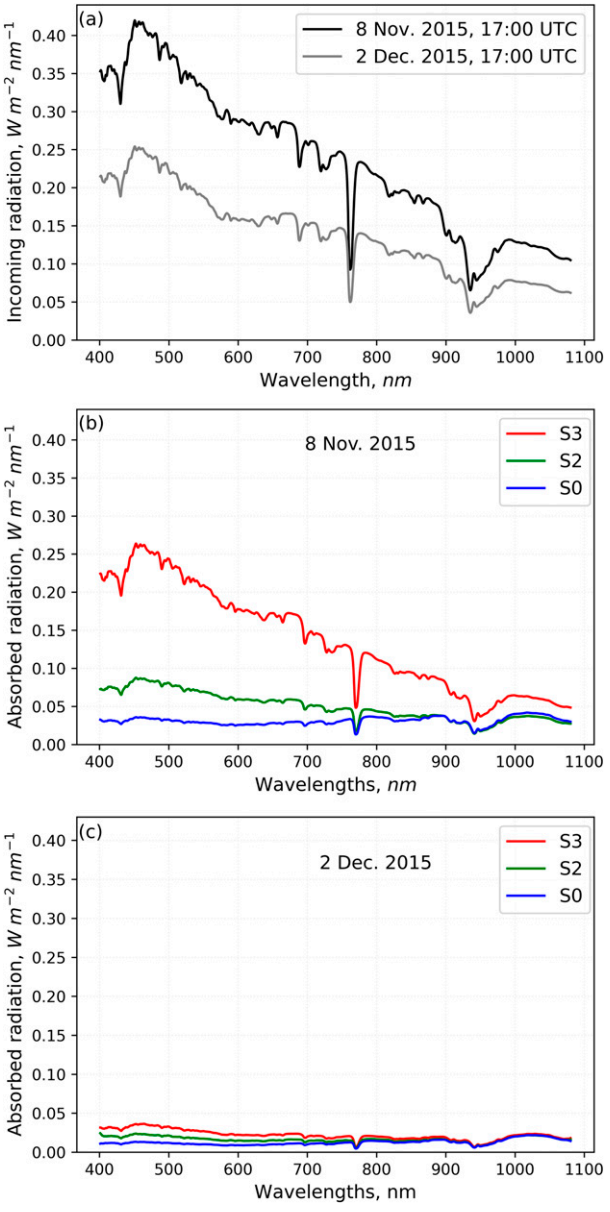

FIG. 10. Spectral incoming radiation as calculated with SBDART and the corresponding spectra of absorbed radiation at the lichen site S0 (blue), medium shrub site S2 (green), and tall shrub site S3 (red). (a) Incoming radiation for 8 Nov and 2 Dec at 1700 UTC for overcast conditions. Spectra of absorbed radiation for 8 Nov are shown in (b) and those for 2 Dec in (c).

that most additional absorption is localized in branches that consequently heat up. As a first consequence, branch heat up increases surface temperatures, which could modify the land surface–atmosphere energy exchange compared to pure snow, affect air temperature, and establish a biogeophysical feedback to climate (Sturm et al. 2005; Pomeroy et al. 2006; Loranty and Goetz 2012). Second, branch heat up may affect the heat

flux through the snow and therefore the thermal regime of permafrost by impacting melting events, snow metamorphism, and depth hoar formation in autumn, which determine the insulating properties of the snowpack that persist all winter (Domine et al. 2016; Barrere et al. 2018). In particular during warm spells, which are becoming more frequent in autumn (Hansen et al. 2014), heated branches locally amplify snow melting (Fig. 5a) and increase the formation of melt–freeze layers in the snowpack (Barrere et al. 2018). Melt–freeze layers have high thermal conductivity (Domine et al. 2016; Barrere et al. 2018) and are therefore poor insulators contributing to permafrost cooling in winter (Barrere et al. 2018). When it is too cold for melting, a horizontal temperature gradient establishes between heated branches and colder snow, which enhances depth hoar formation near branches. Depth hoar usually has a low thermal conductivity and is a good insulator (Domine et al. 2012, 2016), limiting permafrost cooling during winter. However, the radiative effect is locally limited and the most important factor for enhanced depth hoar formation in shrubs is probably due to the lack of snow compaction described in Domine et al. (2016). In conclusion, the temperature evolution in the Arctic tundra and the concomitant frequency of melting events seems to be the controlling factor for the magnitude of the impact of shrub-induced albedo reductions and branch heat up on climate and on the thermal regime of permafrost.

b. *Shrub impact on snow–wind–melt interactions and SSA*

Shrub-induced increases in melting during warm spells and preferential accumulation of wind-driven snow in cold weather have been observed here and in numerous studies (e.g., Sturm et al. 2001; Marsh et al. 2010; Domine et al. 2016). This suggests that snow SSA at the surface, which is influenced by melting and wind-driven redistribution (Domine et al. 2012), is modified by protruding branches. On 8 November, SSA distribution at S0, S2, and S3 was complex (Fig. 6a), probably due to the combined effect of high temperatures and rain on 6 and 7 November, a blizzard in the night of 7/8 November and sunshine on 8 November. SSA at S3 was low (5–15 $m^2 kg^{-1}$), likely because rain and high temperatures on 6 and 7 November produced a melt–freeze layer. It is, however, difficult to understand why SSA did not increase after the blizzard, which had been the case at S2 where SSA is higher (62 $m^2 kg^{-1}$ at the surface) and, to a lesser extent, at S0 (42 $m^2 kg^{-1}$ at the surface). A possible explanation is the sunshine in the morning of 8 November that may have caused radiative heating of branches, which, at S3, where the branch network is densest, melted the snow layer that precipitated during the blizzard. On 15 November, after strong winds, SSA was lower at S0 (~10 $m^2 kg^{-1}$) than at S1, S2, and S3 (61–78 $m^2 kg^{-1}$ at the surface; Fig. 6b), which is the expected distribution because protruding branches increase aerodynamic roughness, reduce wind speed (Essery and Pomeroy 2004; Beringer et al. 2005), and cause fresh snow with high SSA to accumulate whereas at pure snow surfaces fresh snow is scrapped off exposing the underlying melt–freeze crust with low SSA. Before 22 November, temperatures were below freezing and fresh snow precipitated without wind. These conditions caused no particular shrub-induced snow–wind–melting interactions and the corresponding SSA profiles had similarly high values at all sites (64–89 $m^2 kg^{-1}$; Fig. 6c).

The presented data highlight important and complex shrub–SSA interactions, but more detailed measurements are needed to fully understand and quantify the SSA–shrub–albedo effect. Studying shrub–SSA interactions is important because SSA controls the near-infrared albedo of snow (e.g., Dumont et al. 2017) and thus impacts the radiation budget of snow and snowpack temperatures in autumn.

c. *Suitability of LME to model mixed surface albedo*

Overall, observed and calculated mixed surface albedo matched well with a mean RMSE of 0.009 (Fig. 8). The essential preparative step to obtain a good match was to correct artifacts in measured albedo through a scaling factor A. This factor A was consistently between 0.96 and 0.97, except for one day (Fig. 7b), suggesting a systematic error probably caused by the shadow cast by the operator and measuring device. We performed calculations of the shadow in the footprint of the sensor (set at 1 m above the snow surface) due to the operator modeled as a fully absorptive vertical rectangle (200 cm high and 60 cm wide) at a given distance from the sensor. Results show shadowing factors ranging from 0.962 to 0.976 for distances of 1.5–2 m, which agree well with our A factors. Note that the presented LME validation is restricted to diffuse conditions as direct light complicates the problem because χ becomes a function of the solar zenith angle.

Best fits were found using branch albedo α_{veg} measured by Juszak et al. (2014) (Fig. 3), which appears strange because it was measured in Siberia on *Betula nana* shrubs while our study was conducted in the eastern Canadian Arctic with *Betula glandulosa* shrubs. Juszak et al. (2014) used a contact probe, which possibly acquired more representative branch albedo than our hemispherically integrated measurements, which record a bulk signal of branches, some remaining leaves, and

the understory. This underlines the importance of obtaining pure branch albedo spectra.

Overall, using α_{sn_obs} or α_{sn_TARTES} had little influence on the fit quality despite the possible difference of SSA in snow in presence of branches. Measuring snow albedo over adjacent pure snow surfaces, like S0 here, therefore in most cases seems an acceptable approximation to determine α_{sn}. Exceptions are periods with extreme weather conditions, like warm spells or extreme winds, when surface SSA at mixed surfaces varied significantly from SSA at pure snow surfaces. Those conditions are expected to become more frequent in the Arctic with climate warming (Hansen et al. 2014). The performance of simulations with α_{sn_TARTES} may have been biased by our assumption that SSA profiles measured at one point were representative for the whole site area because snow SSA varies in space, especially under windy conditions (Domine et al. 2002) and probably when heated branches cause local melting.

Additional assumptions for the calculation of α_{sn_TARTES} were that impurities were negligible, that SSA and density were correlated and that conditions were 100% overcast. The impurity assumption may seem unlikely as waste burning around Umiujaq provides a source for soot and strong winds could transport mineral dust to the snow. However, if there was an impact of those impurities it was probably included in the coefficient A and the correct determination of quantity and type of impurities would require to sample and analyze the snow or to use vertical absorption profiles (Tuzet et al. 2019), which was beyond the scope of this paper. That SSA and snow density were correlated was shown by an empirical dataset of simultaneously measured density and SSA values (Fig. 2) and has in general been observed elsewhere (Domine et al. 2007). Although the measured density values had relatively large standard deviations, which introduces an uncertainty to the calculated snow density, the impact on snow albedo simulations is probably small in most cases. Snow density impacts snow albedo only indirectly by changing the penetration depth of light (Libois et al. 2013), which limits the impact to specific cases when the surface snow layer has high SSA values and is underlain by a layer with low SSA values. Finally, the assumption of 100% overcast conditions can be considered legitimate because it was based on synoptic observations in the field. Moreover, already small amounts of direct light increased measured snow albedo above 1, which was therefore easily detectable, and, in those cases, measurements were not considered. In summary, the assumption that SSA is spatially homogeneous has probably the strongest impact on the albedo simulations here. The impact of impurities, which is probably small, is absorbed by fitting A and the uncertainty in snow density most likely has a comparatively small impact. We suggest, therefore, that future studies take several measurements of surface SSA for α_{sn_TARTES} calculations to cover spatial variability and to potentially increase the performance of the LME.

5. Conclusions

Shrub-induced decreases of mixed surface albedo are wavelength dependent and, early in the snow season (here 8 November), as high as 55% at 500 nm and 18% at 1000 nm. In autumn, these albedo decreases lead to the additional absorption of 70 $W m^{-2}$ (integrated over 400–1080 nm). The energy is mostly absorbed by protruding branches resulting in radiative branch heating that potentially feeds back on climate by modifying the land surface–atmosphere energy exchange and by increasing air temperatures. By enhancing snow melting during warm spells, branch heating also impacts the insulation properties of snow in autumn, which is an important factor for the thermal regime of permafrost. Snow melting, as well as the preferential accumulation of wind-driven snow in shrubs, modified surface SSA, which is a controlling factor for near-infrared snow albedo and has therefore an impact on the snow radiation budget and snow temperatures in autumn. The evolution of air temperature and the frequency of melting events with climate warming will be the deciding factor on the magnitude of the shrub–albedo effect on climate and the thermal regime of permafrost.

Shrub-induced decreases of mixed surface albedo under diffuse light conditions can be accurately simulated with a linear mixing equation. It is important to use branch albedo instead of hemispherical albedo measured over shrubs in autumn. Simulations using snow albedo measured over adjacent shrub-free sites were satisfyingly accurate (mean RMSE: 0.012) but failed during extreme weather conditions and we suggest instead to calculate snow albedo with TARTES as a function of several snow SSA measurements in shrubs.

Acknowledgments. This work was funded by the BNP Paribas foundation (APT project), NSERC through the discovery grant program to FD and the French Polar Institute (IPEV) through program 1042 to FD. We thank the community of Umiujaq for their hospitality and support in the field. We are also grateful to the Centre d'Études Nordiques (CEN) for providing and maintaining the Umiujaq Research Station. Inge Juszak kindly supplied detailed spectral data of branch albedo, shown in Fig. 3.

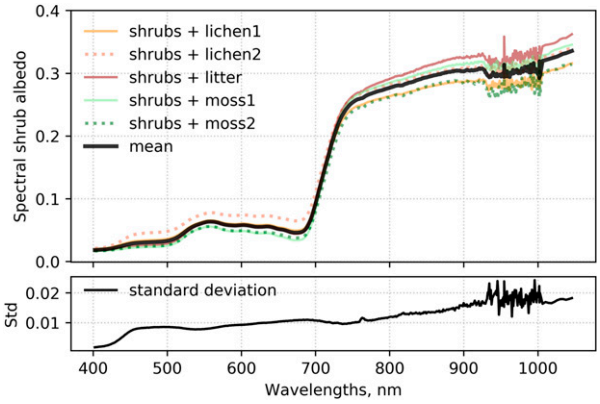

FIG. A1. Spectral shrub albedo measured during the late-summer campaign 2015 for shrubs growing on lichen (two measurements), moss (two measurements), or soil covered by fallen leaves (litter, one measurement).

APPENDIX

Spectral Shrub Albedo Measured near Umiujaq

Figure A1 shows 5 spectral albedo measurements for shrubs with different understory that were acquired near Umiujaq with the Solalb instrument. Measurements were taken during the late-summer campaign in 2015, which took place before the first snow fall but when the shrubs were almost leaf free.

REFERENCES

Barrere, M., F. Domine, M. Belke-Brea, and D. Sarrazin, 2018: Snowmelt events in autumn can reduce or cancel the soil warming effect of snow–vegetation interactions in the Arctic. *J. Climate*, **31**, 9507–9518, https://doi.org/10.1175/JCLI-D-18-0135.1.

Beringer, J., F. S. Chapin, C. C. Thompson, and A. D. McGuire, 2005: Surface energy exchanges along a tundra-forest transition and feedbacks to climate. *Agric. For. Meteor.*, **131**, 143–161, https://doi.org/10.1016/j.agrformet.2005.05.006.

Bonfils, C. J. W., T. J. Phillips, D. M. Lawrence, P. Cameron-Smith, W. J. Riley, and Z. M. Subin, 2012: On the influence of shrub height and expansion on northern high latitude climate. *Environ. Res. Lett.*, **7**, 015503, https://doi.org/10.1088/1748-9326/7/1/015503.

Cabanes, A., L. Legagneux, and F. Domine, 2003: Rate of evolution of the specific surface area of surface snow layers. *Environ. Sci. Technol.*, **37**, 661–666, https://doi.org/10.1021/es025880r.

CEN, 2016: Climate station data from the Umiujaq region in Nunavik, Quebec, Canada, v. 1.3 (1997–2015). Centre d'Études Nordiques, Nordicana D9, https://doi.org/10.5885/45120SL-067305A53E914AF0.

Domine, F., A. Cabanes, and L. Legagneux, 2002: Structure, microphysics, and surface area of the Arctic snowpack near Alert during the ALERT 2000 campaign. *Atmos. Environ.*, **36**, 2753–2765, https://doi.org/10.1016/S1352-2310(02)00108-5.

——, A. S. Taillandier, S. Houdier, F. Parrenin, W. R. Simpson, and T. A. Douglas, 2007: Interactions between snow metamorphism and climate: Physical and chemical aspects. *Physics and Chemistry of Ice*, W. F. Kuhs, Ed., Royal Society of Chemistry, 27–46.

——, ——, A. Cabanes, T. A. Douglas, and M. Sturm, 2009: Three examples where the specific surface area of snow increased over time. *Cryosphere*, **3**, 31–39, https://doi.org/10.5194/tc-3-31-2009.

——, J. C. Gallet, J. Bock, and S. Morin, 2012: Structure, specific surface area and thermal conductivity of the snowpack around Barrow, Alaska. *J. Geophys. Res.*, **117**, D00R14, https://doi.org/10.1029/2011JD016647.

——, M. Barrere, and S. Morin, 2016: The growth of shrubs on high Arctic tundra at Bylot Island: Impact on snow physical properties and permafrost thermal regime. *Biogeosciences*, **13**, 6471–6486, https://doi.org/10.5194/bg-13-6471-2016.

Dumont, M., L. Arnaud, G. Picard, Q. Libois, Y. Lejeune, P. Nabat, D. Voisin, and S. Morin, 2017: In situ continuous visible and near-infrared spectroscopy of an alpine snowpack. *Cryosphere*, **11**, 1091–1110, https://doi.org/10.5194/tc-11-1091-2017.

Essery, R., and J. Pomeroy, 2004: Vegetation and topographic control of wind-blown snow distributions in distributed and aggregated simulations for an Arctic tundra basin. *J. Hydrometeor.*, **5**, 735–744, https://doi.org/10.1175/1525-7541(2004)005<0735:VATCOW>2.0.CO;2.

Gallet, J.-C. C., F. Domine, C. S. Zender, and G. Picard, 2009: Measurement of the specific surface area of snow using infrared reflectance in an integrating sphere at 1310 and 1550 nm. *Cryosphere*, **3**, 167–182, https://doi.org/10.5194/tc-3-167-2009.

Grégoire, M., and Y. Bégin, 1993: The recent development of a mixed shrub and conifer community on a rapidly emerging coast (eastern Hudson Bay, subarctic Québec, Canada). *J. Coast. Res.*, **9**, 924–933.

Hansen, B. B., and Coauthors, 2014: Warmer and wetter winters: Characteristics and implications of an extreme weather event in the High Arctic. *Environ. Res. Lett.*, **9**, 114021, https://doi.org/10.1088/1748-9326/9/11/114021.

Juszak, I., A. M. Erb, C. Maximov, and G. Schaepman-Strub, 2014: Arctic shrub effects on NDVI, summer albedo and soil shading. *Remote Sens. Environ.*, **153**, 79–89, https://doi.org/10.1016/j.rse.2014.07.021.

Lee, W.-L., K. Liou, and A. Hall, 2011: Parametrization of solar fluxes over mountain surfaces for application to climate models. *J. Geophys. Res.*, **116**, D01101, https://doi.org/10.1029/2010JD014722.

Libois, Q., G. Picard, J. L. France, L. Arnaud, M. Dumont, C. M. Carmagnola, and M. D. King, 2013: Influence of grain shape on light penetration in snow. *Cryosphere*, **7**, 1803–1818, https://doi.org/10.5194/tc-7-1803-2013.

Liston, G. E., J. P. Mcfadden, M. Sturm, and R. A. Pielke, 2002: Modelled changes in Arctic tundra snow, energy and moisture fluxes due to increased shrubs. *Global Change Biol.*, **8**, 17–32, https://doi.org/10.1046/j.1354-1013.2001.00416.x.

Loranty, M. M., and S. J. Goetz, 2012: Shrub expansion and climate feedbacks in Arctic tundra. *Environ. Res. Lett.*, **7**, 011005, https://doi.org/10.1088/1748-9326/7/1/011005.

——, ——, and P. S. A. Beck, 2011: Tundra vegetation effects on pan-Arctic albedo. *Environ. Res. Lett.*, **6**, 029601, https://doi.org/10.1088/1748-9326/6/2/029601.

Marsh, P., P. Bartlett, M. MacKay, S. Pohl, and T. Lantz, 2010: Snowmelt energetics at a shrub tundra site in the western Canadian Arctic. *Hydrol. Processes*, **24**, 3603–3620, https://doi.org/10.1002/hyp.7786.

Ménard, C. B., R. Essery, and J. Pomeroy, 2014: Modelled sensitivity of the snow regime to topography, shrub fraction and shrub height. *Hydrol. Earth Syst. Sci.*, **18**, 2375–2392, https://doi.org/10.5194/hess-18-2375-2014.

Myers-Smith, I. H., and Coauthors, 2011: Shrub expansion in tundra ecosystems: Dynamics, impacts and research priorities. *Environ. Res. Lett.*, **6**, 045509, https://doi.org/10.1088/1748-9326/6/4/045509.

Painter, T. H., N. P. Molotch, M. Cassidy, M. Flanner, and K. Steffen, 2007: Contact spectroscopy for determination of stratigraphy of snow optical grain size. *J. Glaciol.*, **53**, 121–127, https://doi.org/10.3189/172756507781833947.

Payette, S., 1976: Les limites écologiques de la zone hémi-arctique entre la mer d'Hudson et la baie d'Ungava, Nouveau-Québec. *Cah. Geogr. Que.*, **20**, 347–364, https://doi.org/10.7202/021325AR.

Pearson, R. G., S. J. Phillips, M. M. Loranty, P. S. Beck, T. Damoulas, S. J. Knight, and S. J. Goetz, 2013: Shifts in Arctic vegetation and associated feedbacks under climate change. *Nat. Climate Change*, **3**, 673–677, https://doi.org/10.1038/nclimate1858.

Picard, G., Q. Libois, and L. Arnaud, 2016a: Refinement of the ice absorption spectrum in the visible using radiance profile measurements in Antarctic snow. *Cryosphere*, **10**, 2655–2672, https://doi.org/10.5194/tc-10-2655-2016.

——, ——, ——, G. Verin, and M. Dumont, 2016b: Development and calibration of an automatic spectral albedometer to estimate near-surface snow SSA time series. *Cryosphere*, **10**, 1297–1316, https://doi.org/10.5194/tc-10-1297-2016.

Pomeroy, J. W., and Coauthors, 2006: Shrub tundra snowmelt. *Hydrol. Processes*, **20**, 923–941, https://doi.org/10.1002/hyp.6124.

Provencher-Nolet, L., M. Bernier, and E. Lévesque, 2014: Short term change detection in tundra vegetation near Umiujaq, subarctic Quebec, Canada. *Geoscience and Remote Sensing Symposium (IGARSS)*, Quebec City, QC, Canada, IEEE, https://doi.org/10.1109/IGARSS.2014.6947534.

Ricchiazzi, P., S. Yang, C. Gautier, and D. Sowle, 1998: SB DART: A research and teaching software tool for plane-parallel radiative transfer in the Earth's atmosphere. *Bull. Amer. Meteor. Soc.*, **79**, 2101–2114, https://doi.org/10.1175/1520-0477(1998)079<2101:SARATS>2.0.CO;2.

Ropars, P., and S. Boudreau, 2012: Shrub expansion at the forest–tundra ecotone: spatial heterogeneity linked to local topography. *Environ. Res. Lett.*, **7**, 015501, https://doi.org/10.1088/1748-9326/7/1/015501.

Sturm, M., J. P. Mcfadden, G. E. Liston, F. S. Chapin III, C. H. Racine, and J. Holmgren, 2001: Snow–shrub interactions in Arctic tundra: A hypothesis with climatic implications. *J. Climate*, **14**, 336–344, https://doi.org/10.1175/1520-0442(2001)014<0336:SSIIAT>2.0.CO;2.

——, T. Douglas, C. Racine, and G. Liston, 2005: Changing snow and shrub conditions affect albedo with global implications. *J. Geophys. Res.*, **110**, G01004, https://doi.org/10.1029/2005JG000013.

Taillandier, A. S., F. Domine, W. R. Simpson, M. Sturm, and T. A. Douglas, 2007: Rate of decrease of the specific surface area of dry snow: Isothermal and temperature gradient conditions. *J. Geophys. Res. Earth Surf.*, **112**, F03003, https://doi.org/10.1029/2006JF000514.

Tape, K., M. Sturm, and C. Racine, 2006: The evidence for shrub expansion in northern Alaska and the pan-Arctic. *Global Change Biol.*, **12**, 686–702, https://doi.org/10.1111/j.1365-2486.2006.01128.x.

Tuzet, F., M. Dumont, L. Arnaud, D. Voisin, M. Lamare, F. Larue, J. Revuelto, and G. Picard, 2019: Influence of light-absorbing particles on snow spectral irradiance profiles. *Cryosphere*, **13**, 2169–2187, https://doi.org/10.5194/tc-13-2169-2019.

Vionnet, V., G. Guyomarc'h, F. Naaim Bouvet, E. Martin, Y. Durand, H. Bellot, C. Bel, and P. Puglièse, 2013: Occurrence of blowing snow events at an alpine site over a 10-year period: Observations and modelling. *Adv. Water Resour.*, **55**, 53–63, https://doi.org/10.1016/j.advwatres.2012.05.004.

Warren, S. G., 1982: Optical properties of snow. *Rev. Geophys. Space Phys.*, **20**, 67–89, https://doi.org/10.1029/RG020i001p00067.

——, and R. E. Brandt, 2008: Optical constants of ice from the ultraviolet to the microwave: A revised compilation. *J. Geophys. Res.*, **113**, D14220, https://doi.org/10.1029/2007JD009744.